NUMERICAL STUDY OF TIME-DEPENDENT HYGROTHERMAL CONDITIONS IN DEPRESSURIZED CRAWL SPACE

Juha Salo[1], Petteri Huttunen[1], Juha Vinha[1], Timo Keskikuru[1]

[1]TUT, Tampere University of Technology, P.O. Box 527, FI-33101 Tampere, Finland

petteri.huttunen@tut.fi

Acknowledgements

This project was funded by Finnish Ministry of The Environment (operational programme: *Kosteus- ja hometalkoot*), which is gratefully acknowledged.

Blinded Manuscript Click here to view linked References

Abstract

A finite element based hygrothermal model consisting of several interconnected components with varying number of spatial dimensions was applied to analyze the time-dependent temperature and humidity conditions of a mechanically depressurized and ventilated crawl space. Purpose of the depressurization is to prevent the intrusion of radon or other insanitary particles into indoor air. However, in typical foundation structures the depressurization will cause air flow from soil into the crawl space air and it may convey excessive moisture making the hygrothermal conditions potential for mould growth or other moisture-induced biological damage, which is not considered to be acceptable even with the depressurization. Although in general the forced convection of humidity from soil presumably increases relative humidity in crawl space, significant heat capacity of the ground may warm the air flowing into the crawl space and thus decrease the relative humidity. Overall effect of the depressurization on the conditions in crawl space is therefore not trivial. Because a full-scale three-dimensional finite element analysis of heat, mass and momentum transfer in crawl space and its surroundings would require excessive computational resources, several simplifications were necessary to apply in the model. According to the numerical results, the airflow through drainage layer into crawl space does not seem to have severe effect on the crawl space conditions. Conversely, in cold periods the relative humidity in crawl space is very low because of the air temperature is increased while flowing through the drainage layer.

Keywords: crawl space, depressurization, multicomponent hygrothermal model, COMSOL Multiphysics

List of symbols

$A_{base\ floor}$ floor area of the base floor (m^2)

A_{ground} floor area of the ground of the crawl space (m^2)

A_{fw} foundation wall surface area (m^2)

c_p specific heat capacity at constant pressure (J/kg·K))

D_v water vapour diffusion coefficient (m^2/s)

D_w liquid transport coefficient (m^2/s)

$G_{base\ floor}$ diffusive moisture flow between crawl space and surface of base floor (kg/s)

$G_{condense}$ term for forming liquid water of possible water vapour condensation (kg/s)

G_{ext} convective moisture flow carried by outward airflow from crawl space to open air (kg/s)

$G_{ground,conv}$ convective moisture flow to crawl space carried by inward airflow through drainage layer (kg/s)

$G_{ground,diff}$ diffusive moisture flow between crawl space and surface of ground structure (kg/s)

G_{out} convective moisture flow carried by inward airflow directly from outdoor to crawl space (kg/s)

ΣG_{in} sum of the inward moisture flows (kg/s)

ΣG_{out} sum of the outward moisture flows (kg/s)

h_{bf} heat transfer coefficient between the lower surface of the base floor and crawl space ($W/(m^2 \cdot K)$), in this study 10 $W/(m^2 \cdot K)$

h_{fw} heat transfer coefficient between foundation wall inner surface and crawl space ($W/(m^2 \cdot K)$), in this study 10 $W/(m^2 \cdot K)$

h_{ground} heat transfer coefficient between ground surface and crawl space (W/(m^2·K)), in this study 10 W/(m^2·K)

h_v evaporation heat of water, ≈ 2260 (MJ/kg)

$p_{v,sat}$ water vapour saturation pressure (Pa)

P_{eff} effective perimeter (m)

R_{ground} volume flow through aggregate gravel (m^3/s)

R_{out} volume flow of replacement air from outdoor to the crawl space (m^3/s)

R_{2D} volume flow through drainage layer in 2D-model (m^3/s)

R_{3D} volume flow through drainage layer in 3D-model (m^3/s)

R_w specific gas constant of water, 461.5 J/(kg·K)

S_v source term related to condensation rate kg/(m^3·s)

T temperature (K)

T_{bf} temperature of the lower surface of base floor (K)

T_{ground} average surface temperature of the ground structure of the crawl space(°C)

T_{out} outdoor temperature (°C)

T_{fw} average foundation wall surface temperature (°C)

$\boldsymbol{u}$ Darcy velocity (m/s) or in general velocity vector (m/s)

V_{cs} volume of the crawl space (m^3)

w moisture content (kg/m^3)

β_{bf} mass transfer coefficient between base floor lower surface and crawl space (m/s), in this study 3e-3 m/s

β_{ground} average mass transfer coefficient between ground surface and crawl space (m/s), in this study 3e-3 m/s

δ_p water vapour permeability of the building material (kg/(m·s·Pa))

κ air flow permeability of the porous medium (m^2)

λ thermal conductivity (W/(m·K))

μ the dynamic viscosity of the fluid (kg/(m·s)) or water vapour resistance factor (-)

ν_{bf} water vapour concentration at the lower surface of the base floor (kg/m^3)

ν_{cs} water vapour concentration in crawl space (kg/m^3)

ν_{ground} average water vapour concentration at the surface of the floor of the crawl space (kg/m^3)

$\nu_{sat}(T)$ vapour saturation concentration, function of temperature (kg/m^3)

ξ moisture storage capacity (kg/m^3)

ρ density (kg/m^3)

Φ_{bf} conductive heat flow between crawl space and lower surface of base floor (W)

$\Phi_{condense}$ term for released heat from possible condensation of vapour (W)

Φ_{exit} convective heat flow carried by outward airflow from crawl space to open air (W)

$\Phi_{ground,cond}$ conductive heat flow to crawl space between crawl space and surface of ground structure (W)

$\Phi_{ground,conv}$ convective heat flow carried by inward airflow through aggregate gravel (W)

Φ_{out} convective heat flow carried by inward airflow directly from outdoor to crawl space (W)

Φ_{fw} heat flow between crawl space and foundation wall (W)

$\Sigma\Phi_i$ sum of heat flows related to crawl space energy balance (W)

ΣG_i sum of vapour mass flows related to crawl space moisture balance (kg/s)

φ is relative humidity (-)

φ_{out} relative humidity of outdoor air (-)

1 Introduction

Radon is a radioactive and carcinogenic gas, which is naturally produced in many soil minerals and its migration into indoor air should be always minimized. An example of preventative measure against radon migration in buildings with crawl space foundation is depressurizing mechanically the crawl space against occupied indoor space. This type of solution has been a subject of interest in earlier Finnish experimental field studies: Keskikuru et al. (1999), Keskikuru et al. (2000a), Keskikuru et al. (2000b) and Keskikuru et al. (2001), and based on the concentration measurements it was found to be a functional way of preventing the unwanted radon migration. However, negative pressure ratio between crawl space and indoors (and outdoors) may cause hygrothermally harmful airflows from outdoors to crawl space through soil and drainage layer if the bottom of the crawl space is not airtight. Obviously, this type of airflow can convey water vapour from soil moisture into crawl space and

result in increased relative humidity. Depending on the season, however, the thermal capacity of soil together with the upward heat flux from Earth's interior may also increase the temperature of flowing air and thus also warm up the crawl space, which – on the contrary – may occasionally result in decreased relative humidity compared to outdoor air or non-depressurized crawl space. The overall effect of mechanical depressurization on the convenience of hygrothermal conditions in crawl space for mould growth (or other biological damaging in humid conditions) is thus clearly non-trivial and may be different depending on the season. Although sufficient pressure difference can prevent radon and other insanitary substances (like mould toxins) intrusion to living space, continuously critical conditions in crawl space are not considered acceptable. Subject of this study was solely the hygrothermal conditions in depressurized crawl space, not its ability to maintain low radon concentration in living spaces. The study is part of the finalization of co-author Lic.Phil. Keskikuru's dissertation.

Numerical modelling was used in this study to analyze time-dependent hygorthermal conditions in ideally depressurized and ventilated crawl space with different constant ventilation rates. In principle, a mechanical system, which regulates the depressure to a desired level, could be based on an exhaust blower, which rotating speed is adjusted frequently by a microcontroller and a pressure difference transmitter so that the desired pressure difference is maintained. In addition, if the depressurization system is ideal in the sense that it can maintain desired constant depressure regardless of the airflow rate through the exhaust blower, the foundation wall can be fitted with a number of adjustable ventilation valves (e.g. iris valves with pneumatic connections for pressure difference measurement, adjustable aperture size and accurately known pressure drop per flow rate -curve) so that the total ventilation rate per certain pressure difference can be throttled to a desired level. In reality, however, this type of setup would certainly have time-dependent fluctuations in flow rates and pressure differences to some extent, but for the sake of simplicity in this study the boundary conditions were

restricted to represent ideal depressurization system with constant pressure difference and different constant ventilation rates. Air change rate due to pressure difference was assumed to contain no leakages from indoor air. Air leakages from living space would presumably increase the relative humidity in unheated crawl space every season because of the indoor moisture excess. This possible effect was, however, decidedly excluded from the computations so that only the effect of ground and airflows through drainage layer could be analyzed. In addition, typical airtightness between living space and crawl space or its deviation in existing buildings is hard to approximate without extensive experimental data.

By using real climate data as boundary conditions, time-dependent values for the average temperature and relative humidity in the crawl space air were solved numerically. The effect of depressurization on the risk of mould growth in crawl space was finally evaluated simply by counting and comparing the number of time instants (step size 1 hour) when the mould growth in building materials is possible (i.e. temperature > 0 °C, relative humidity > 80 % RH, Hukka & Viitanen (1999)) to the corresponding number of time instants in outdoor air i.e. the climate data used in boundary conditions. By this way it is possible to get rough estimate of the overall hygrothermal functionality of the depressurization system and to attempt to get answers to the following questions: do the airflows through drainage layer enhance or reduce the moisture-safety of the crawl space in general, how does it depend on season and what is the optimal ventilation rate?

Coupled numerical model consisted of energy and mass balance equations of the crawl space air, which was assumed to be perfectly mixed and which was connected to finite element models of surrounding ground and foundation structures. Certain other simplifcations related to the modelling of surrounding structures were also necessary and they are described in the chapter 2. Altogether, the

model consisted of multiple interconnected components and is hereafter called a multicomponent hygrothermal model (denoted by MCHTM) and it was assembled and solved in multiphysical finite element software suite COMSOL Multiphysics.

1.1 Earlier studies and model basis

Crawl space depressurization is described in Henschel (1992) as an alternative to better-known sub-membrane depressurization (SMD) method where the crawl space bottom is covered with impearmeable membrane and the depressurization is applied beneath the membrane. Low installation costs are mentioned as advantages of the crawl space depressurization compared to SMD, but the SMD is described as more reliable for ensuring low radon concentrations in living spaces. Although the method is introduced at least two decades ago and its usefulness in radon control has been a subject of interest, earlier experimental or numerical studies, where the long-term effect of depressurization on unsealed crawl space's time-dependent hygrothermal conditions are explicitly on the main focus, were not found from literature. However, partially or distinctively similar numerical studies, where either sub-surface airflows in soil due to active radon control system or time-dependent crawl space hygrothermal conditions are modelled, can be found and the MCHTM was compiled by following as closely as possible the same principles and assumptions deemed appropriate and applied in earlier studies.

Forced airflows in ground were modelled according to linear Darcy's law at least in e.g. Jiranek & Svoboda (2007) and more recently in Diallo et al. (2015). Nonlinear Forcheimer term, which describes the inertial effect of the gas itself on the relation between flow velocity and pressure gradient, should be taken into account when the Reynolds number is clearly above 10 [-] (Zeng &

Grigg (2006)). However, because accurate computation of Reynolds number would require knowledge of average hydraulic diameter inside gravel and the possible effect of inertia was assumed to be negligible, for the sake of simplicity airflow fields in this study were modelled by linear Darcy's law for incompressible flow.

Even though three-dimensional time-independent radon transport in soil with forced convection (according to linear Darcy's law) has been previously modelled successfully in e.g. Jiranek & Svoboda (2007), it is obvious that introducing time-dependency to the problem and attempting to model the seasonal hygrothermal behaviour in large domains – such as ground beneath a building – with small time steps compared to the total simulation period will expand the computational costs exponentially and make the modelling numerically very challenging or even impossible, at least without high-performance computing experience and resources. For this reason, convective-diffusive transport of heat and water vapour in drainage layer was modelled here in 2D domain, which was connected with the crawl space model with so called effective perimeter (explained in chapter 2).

Similar problem arises even more with the long-term coupled CFD modelling of temperature, humidity and turbulent velocity fields in ventilated crawl spaces: in principle it is possible, but often too costly and would also involve laborious post-processing of the results. Moreover, the accuracy of the physical model could be improved further, e.g. by taking into account the explicit radiation balance between interior surfaces of the crawl space, which would possibly increase the nonlinearity of the model dramatically and make the computations yet challenging.

In order to analyze the risk of biological damaging in buildings, however, either long-term measurements or simulations are required anyway since the possible damaging happens slowly (in years or even in decades). MCHTM used in this study was compiled by complying with same principle applied in Matilainen & Kurnitski (2003), according to which the crawl space can be modelled as a single component belonging to larger network of components (RC-network). In practice this means that the crawl space air is assumed to be constantly fully mixed, i.e., the distribution of temperature and humidity in crawl space is even. Hygrothermal conditions in crawl space is thus mathematically treated as lumped system and its state is determined by two variables (temperature and humidity). This principle has been applied also in the modelling of pollutant transport in indoor air (Diallo et al. (2015)) reportedly with satisfactory results compared to experimental data.

2 Model details

MCHTM consisted of three different components: crawl space, base floor and ground and foundation structures. Base floor structure between crawl space and indoor air was modeled as one-dimensional structure, while the temperature and humidity in foundations and soil around and between the crawl space was modeled in 2D domains. Because the pressure difference was assumed to be constant, time-independent airflow field was first solved and used as initial data for time-dependent modelling of convective-diffusive transport of heat and water vapour. 10 Pa absolute value was chosen for the depressure magnitude in every computation; it was approximated to be large enough for the preventation of radon entry into indoor, but not too large energy-efficiency-wise and in the view of excess moisture convection into crawl space.

2.1 Studied structures

Three different cases were modelled: a crawl space where the bottom was uncovered and the lower drainage layer had two different permeabilities, and an airtight crawl space where the bottom was covered with 50 mm concrete layer.

In Fig. 1, foundation base (1) consisted of concrete and foundation wall (2) consisted blocks of expanded clay aggregate. Ground frost insulation of foundation (3) consisted of rigid thermal insulation (expanded polystyrene EPS). Drainage layer of the foundation (4) consisted of aggregate gravel. The foundation soil (5) is handled as solid material which had constant thermal properties.

In Fig. 2 is illustrated 2D ground and foundation structure of airtight crawl space. In this case the modelling is significantly easier task since the convergence of finite element solutions is faster in the absence of convection.

In Fig. 3 is illustrated the whole studied geometry of ground and foundation structures. The size of foundation soil was chosen as big as feasible in order to model reliably the effect of the thermal capacity of ground.

One-dimensional base floor consisted of a concrete slab (thickness 175 mm) (blank concrete surface towards indoor) and rigid thermal insulation (thickness 220 mm) towards crawl space. Thus,

MCHTM treated the base floor as a infinity wide, constant thick layered structure, where the effect of e.g. coldness at the exterior wall joints in fringe area was not modelled.

2.2 Governing equations, physical assumptions and interconnections between components

For the modelling of convection in drainage layer (in Fig. 1 part 4) the time-independent Darcy's law was first solved:

$$\boldsymbol{u} = -\frac{\kappa}{\mu}\nabla p \tag{1}$$

with the continuity equation:

$$\nabla \cdot \boldsymbol{u} = 0 \tag{2}$$

Pre-solved airflow field $\boldsymbol{u}$ was used as initial data in the time-dependent 2D model of heat and vapour transfer in ground and soil, which was governed by partial differential equations:

$$\rho_{soil} C_{p,soil} \cdot \frac{\partial T}{\partial t} + \rho_{air} C_p \boldsymbol{u} \cdot \nabla T - \nabla \cdot (\lambda_{soil} \nabla T) = h_v \cdot S_v(v, T) \tag{3}$$

$$\frac{\partial v}{\partial t} + \boldsymbol{u} \cdot \nabla v - \nabla \cdot (D_v \nabla v) = -S_v(v, T) \tag{4}$$

Purpose of use of aggregate gravel was to use it as a capillary break between moist foundation soil and building foundation. The used aggregate gravel was assumed to containing non-fine fraction (sand) because of the function of capillary break and it was also assumed to be washed out of dust to avoid moisture storing in the dust. Capillary transport of water in this kind of aggregate gravel (crushed stone with some fine fraction) is negligible (Rantala & Leivo 2007). As can be seen from equation 4, aggregate gravel was modeled without moisture capacity. Rantala & Leivo (2007) have found out that moisture capacity of crushed stone, which includes very little amount of fine fractions,

moisture content during adsorption was very low: at in ambient temperature of 20 °C the maximum value of the hygroscopic equilibrium moisture content of crushed stone during wetting is less than 0.4 %-weight. Based on previous assumptions moisture capacity of aggregate gravel can be assumed negligible.

For the sake of simplicity, in parts other parts than (4) convection and the moisture transport was not modelled, and the only variable to solve for was temperature:

$$\rho C_p \cdot \frac{\partial T}{\partial t} - \nabla \cdot (\lambda \nabla T) = 0 \tag{5}$$

Source terms $h_v \cdot S_v(v,T)$ and $-S_v(v,T)$ were implemented to take into account the occasionally possible effect of condensation, i.e. relative humidity exceeding 100 % RH. Rate of condensation was modelled by a soft limiter function:

$$S_v(v,T) = \begin{cases} 0, \text{if } v < v_{sat}(T) \\ K_v \cdot \left(v - v_{sat}(T)\right), \text{otherwise} \end{cases} \tag{6}$$

where K_v (1/s) is an artificial coefficient related to the rate of condensation. Basically, as large as possible value should be chosen for K_v in order to minimize the occurrence of concentrations higher than temperature-dependent saturation concentration of water vapour in the solution. However, it was found that too large values for K_v will cause numerical problems in achieving convergence with time-dependent solver. Value $K_v = 5$ (1/s) was found out to be suitable and was finally used in all the computations. Temperature-dependent saturation concentration $v_{sat}(T)$ was implemented as a callable function in COMSOL, and it was computed by the well-known ideal gas law, where partial pressure at saturation was approximated by formula proposed in EN ISO 13788:2012. The condensing water vapour was assumed to pour immediately through aggregate gravel to top of the foundation soil which stays constantly at 100 % RH.

Crawl space was connected to surrounding components by using crawl space's temperature and vapour concentration as boundary conditions for surrounding components, and reciprocally computing the entering and leaving fluxes of heat and mass (convective and diffusive terms in equations 1 and 2) from the surrounding components' variables at boundaries with proper integration operators. COMSOL includes built-in coupling operators for different modeling situations, which can be used to connect two or more components and solve them simultaneously, as a one large problem (COMSOL Multiphysics 2016).

Energy and mass (water vapour) balance of the fully mixed crawl space air can be written as:

$$\rho_{air} C_{p,air} V_{cs} \cdot \frac{\partial T_{cs}}{\partial t} = \Sigma \Phi_i \tag{7}$$

$$V_{cs} \cdot \frac{\partial \nu_{cs}}{\partial t} = \Sigma G_i \tag{8}$$

where $\Sigma \Phi_i$ and ΣG_i consist of both convective and diffusive terms, which describe the different factors affecting the temperature and humidity in crawl space air.

Although the crawl space was treated as fully mixed, it was assumed to have physical dimensions, area, hight and volume. Values 129 m^2 (14.5 m x 8.9 m), 0.8 m and 104 m^3 were used in the computations and they correspond to an actual building, which was used in experimental study Keskikuru (1999). Connecting 2D heat and mass transfer simulation of ground into idealized 3D crawl space requires an auxiliary parameter, which is used to multiply the result of boundary integration from 2D domain to determine the volume flow through drainage layer into crawl space. The is called here *effective perimeter* and is denoted by P_{eff} (m). It was solved by first modelling the airflow in drainage layer in both 3D and 2D geometries:

$$P_{eff} = \frac{R_{3D}}{r_{2D}} \quad (9)$$

where R_{3D} (m^3/s) is obtained from 3D model and r_{2D} ($m^3/(s \cdot m)$) from 2D model by using proper integration operators in post-processing. Symmetry was utilized in 3D model. Volume flow is from now on denoted and computed by:

$$R_{3D} = R_{ground} = P_{eff} \cdot r_{2D} \quad (10)$$

Two different values of the permeability of the aggregate gravel of drainage layer: 1e-8 m^2 and 1e-9 m^2. In Fig. 4 is illustrated total velocity in the gravel when constant 10 Pa depressurization when permeability of aggregate gravel is 1e-9 m^2. According to the time-independent 3D simulations, volume flows through aggregate gravel R_{ground} were for permeability of aggregate gravel 1e-8 m^2 0.028 m^3/s and for permeability 1e-9 m^2 0.0028 m^3/s. For uncovered crawl space the total volume air flow which comes into crawl space R_{tot} (m^3/s) consist of replacement air and volume flows through aggregate gravel:

$$R_{tot} = R_{ground} + R_{out} \quad (11)$$

For air-sealed crawl space the total volume flow consisted only of replacement air R_{out}, while $R_{ground} = 0$.

Factor *a* (-) is defined as the ratio between volume flows through aggregate gravel and replacement air:

$$a \equiv \frac{R_{ground}}{R_{out}} \quad (12)$$

Factor *a* is defined here for perceiving the magnitudes of replacement air and volume flow through gravel relative to each other, and it is used in later chapter where results are presented.

Hourly temperature and humidity values of the crawl space were modeled with" *The Global ODEs and DAEs*" module of COMSOL Multiphysics (COMSOL Multiphysics 2016). In this study we were interested in hourly values of the temperature T_{cs} (°C) and relative humidity φ_{cs} (-) values of the crawl space air. Variables in lumped system equations were temperature T_{cs} and water vapour concentration ν_{cs} (kg/m^3) of the crawl space air. In Fig. 5 is illustrated interaction between crawl space and its surroundings.

Terms in RHS of the equations 7 and 8 are thus:

$$\Sigma\Phi_i = \Phi_{out} + \Phi_{ground,cond} + \Phi_{ground,conv} + \Phi_{bf} + \Phi_{fw} + \Phi_{exit} + \Phi_{condense} \quad (13)$$

$$\Sigma G_i = G_{out} + G_{ground,cond} + G_{ground,conv} + G_{bf} + G_{exit} + G_{condense} \quad (14)$$

where Φ_{out} and G_{out} are the heat and vapour mass flows from outdoors due to replacement air:

$$\Phi_{out} = R_{out}\rho_{air}C_{p,air}T_{out} \quad (15)$$

$$\mathrm{G}_{out} = R_{out}\varphi_{out}\nu_{sat}(T_{out}) \quad (16)$$

$\Phi_{ground,cond}$, $\Phi_{ground,conv}$, $G_{ground,diff}$ and $G_{ground,conv}$ are the diffusive and convective heat and vapour mass flows at the crawl space bottom surface:

$$\Phi_{ground,cond} = h_{ground}A_{ground}\left(T_{ground} - T_{cs}\right) \quad (17)$$

$$\Phi_{ground,conv} = P_{eff}\rho_{air}C_{p,air}\int_{CS\ boundary} u_y \cdot T\ \mathrm{ds} \quad (18)$$

$$G_{ground,diff} = \beta_{ground}A_{ground}\left(\nu_{ground} - \nu_{cs}\right) \quad (19)$$

$$G_{ground,conv} = P_{eff} \int_{CS\ boundary} u_y \cdot \nu \, ds \quad (20)$$

Φ_{bf} and G_{bf} are the heat and vapour mass flows between lower surface of the base floor and crawl space:

$$\Phi_{bf} = h_{bf} A_{ground} (T_{bf} - T_{cs}) \quad (21)$$

$$G_{bf} = \beta_{bf} A_{ground} (\nu_{bf} - \nu_{cs}) \quad (22)$$

Φ_{fw} is the heat flow between foundation wall and crawl space.

$$\Phi_{fw} = h_{fw} A_{fw} \quad (23)$$

For the sake of simplicity and because of the limited computational resources, moisture transfer in foundation wall and base was not modelled in order to reduce the number of degrees of freedom, nonlinearity of the whole model and computation times. Exiting heat and vapour mass flows Φ_{exit} and G_{exit} are:

$$\Phi_{exit} = -R_{tot} \rho_{air} C_{p,air} T_{cs} \quad (24)$$

$$G_{exit} = -R_{tot} \nu_{cs} \quad (25)$$

Effect of possible condensation in crawl space air was modelled analogously with the equation 6:

$$\Phi_{condense} = h_v \cdot S_v(\nu_{cs}, T_{cs}) \quad (26)$$

$$G_{condense} = -S_v(\nu_{cs}, T_{cs}) \quad (27)$$

2.2.1 Coupled heat and moisture transfer in base floor and airtightening concrete

Coupled heat and moisture transfer model, which is used e.g. in WUFI simulation software (Künzel 1995), was used in base floor structure and airtightening concrete layer. Implementation of coupled heat and moisture transfer equations was carried out with module" *The Coefficient Form PDE*" of the COMSOL Multiphysics. Nusser & Teibinger (2012) and Williams Portal (2011) were used for implementing the coupled heat and moisture transfer in COMSOL Multiphysics. Used equation for moisture balance was:

$$\xi \frac{\partial \varphi}{\partial t} = \nabla \cdot \left[\delta_p \left(p_{sat} \nabla \varphi + \varphi \frac{\partial p_{sat}}{\partial T} \nabla T \right) + \xi D_w \nabla \varphi \right] \tag{28}$$

and for energy balance:

$$\rho C_p \frac{\partial T}{\partial t} = \nabla \cdot (\lambda \nabla T) + h_v \nabla \cdot \left[\delta_p p_{sat} \nabla \varphi + \delta_p \varphi \frac{\partial p_{sat}}{\partial T} \nabla T \right] \tag{29}$$

Equations of coupled heat and moisture transfer include the effect of moisture capacity of materials which allows model conditions in crawl space more realistic way compared to the modelling of heat and vapour transfer in drainage layer. It was also necessary in order to model the significant effect of moisture capacity of concrete used in air-sealing.

2.3 Boundary conditions

A building physical reference year determined in the Finnish research project called FRAME (Vinha et al. 2013) was was used as outdoor temperature and humidity conditions. Two reference years were determined in the FRAME project: Jokioinen 2004 and Vantaa 2007. It was concluded in the project that two reference years are required in critical building physical analyses in Finnish climate: one for the structures for which the driving rain and its absorption is the critical factor (Vantaa 2007), and

one for the structures for which the almost constantly high relative humidity in outdoor air is critical (Jokioinen 2004), e.g. structures, which are protected against driving rain, but where the hygrothermal conditions in ventilated layers and spaces may be questionable because. Since crawl space as a strucuture fits the latter description, Jokioinen 2004 was used in this project, and the structures were simulated for two years with the same climate data on both years. The possible rainwater was assumed to pour down immediately through aggregate gravel to top of the foundation soil as well as the possible condensed water in drainage layer or crawl space. After several years of constant depressurization it could be possible that the top of the soil beneath the drainage layer dries to lower humidity level than 100 % RH, but this possible effect was neglected so that the analysis would be critical. In Fig. 6 is illustrated outdoor temperature and relative humidity in Jokioinen 2004.

The indoor temperature was constant, 21 °C, year-round. Indoor relative humidity was approximated by moisture excess given in Finnish guide (RIL 107 2012). Value of moisture excess $\Delta\nu$ (difference of water vapour concentration between indoors and outdoors) depends on outdoor temperature. It's maximum value in humidity class II is 5 g/m^3 (when outdoor temperature is $\leq$ 5 °C) and minimum value is 2 g/m^3 (when outdoor temperature is $\geq$ 15 °C). Between outdoor temperatures 5 °C and 15 °C the moisture excess is linearly interpolated.

Deep down from foundation soil rising geothermal heat was taken into account by adding inward heat flux q = 0.03 W/m^2 (Neumann boundary condition) into bottom of the foundation soil. Top of the foundation soil was assumed to stay at water vapour concentration which corresponds to 100 % RH.

2.4 Material properties

Permeability of drainage layer depends strongly on grain size ranges and amounts of fine fractions of the fill gravel. In Table 1 is illustrated different permeabilities and grain sizes of typical Finnish aggregates used with foundation structures of buildings.

Permeabilities of typical Finnish fill gravel material varies between 1e-9…1e-8 m^2 and grain size range is from several millimeters to tens of millimeters (STUK A-252 2012). Based on this, studied permeabilities of aggregate gravel were 1e-8 m^2 and 1e-9 m^2. Another values for permeability of gravel can be found in literature, for instance Gadgil (1992) gives 1e-10…1e-6 m^2, Diallo et al. (2013) 1e-9 m^2, Diallo et al. (2015a) 1e-7 m^2 and Riley et al. (1996) 3e-7 m^2 for permeability of gravel. These values of permeabilities of gravel takes a no stand on grain size or amount of the fine fractions in the gravel. For the foundation soil can be found values of permeabilies such as 1e-11 m^2 (Diallo et al. 2015), 1e-13…1e-11 m^2 (Jiranek & Svoboda 2007) and 6e-14…7e-10 m^2 (Nazaroff 1992). Diallo et al. (2015) have measured permeability 2.61e-13 m^2 for foundation soil. Permeabilities of foundation soil might be several orders of magnitude lower than permeabilities of gravel. Airflows in soil was thus assumed to be negligible and the flow was modelled only in drainage layer.

In Tables 2–7 are presented other material properties which were used in this study.

Water vapour resistance factor μ for aggregate gravel in drainage layer was:

$$\mu = D_{v,air}/D_{v,gravel} \tag{30}$$

where liquid transport coefficient for stagnant air $D_{v,air}$ was 2.5e-5 m^2/s was used (Hagentoft 2001). Diffusion coefficient for gravel $D_{v,gravel}$ was:

$$D_v = \frac{\delta_p}{R_w \cdot T} \tag{31}$$

where Leivo & Rantala (2001) gives for water vapour permeability of aggregate gravel δ_p = 30 kg/(m·s·Pa), which corresponds to relative value μ = 6.25.

2.5 Numerical framework

Modelling work was carried out by commercial finite element method based multiphysical simulation software COMSOL Multiphysics. The software is suitable for multiple interconnected components representing different parts and phenomena interacting with each other. Different physical phenomena set different demands for density and structure of the mesh. In Fig. 8 is illustrated mesh structure of simulation geometry of this study.

As can be seen in Fig. 8, the density of mesh is denser in parts where convention of mass and heat were dominant transfer phenomena. Solving temperature field for foundation soil was used 5 100 triangular elements whereas convection dominant drainage layer was used 49 600 triangular elements instead. Additionally, solving stationary airflow field for 3D structure in Fig. 2 was used 510 000 tetrahedral elements. Time step size was set to be freely chosen by the software, but with maximum value of 1 hour.

Because the solution of convection-diffusion equation may be unstable when standard Galerkin element method is applied, a numerical stabilization technique is necessary (Zienkiewicz et al. 2013). Built-in options in COMSOL Multiphysics (version 5.2a) module *Transport of Diluted Species* for consistent numerical stabilization are streamline and crosswind diffusion, and were both applied in the computations. Do Carmo and Galeão as crosswind diffusion type for free flow was found to be

more efficient than the other available option (Codina) and was applied in the computations. (COMSOL Multiphysics (2016))

3 Results

Because of vast amount of numerical result data produced by the MCHTM, we focus only on time-dependent conditions in crawl space and show only few examples of temperature and humidity fields in 2D domains. Two different types of crawl space structure were studied: uncovered ground and air-sealed ground (bottom of the crawl space). In uncovered cases two different types of permeabilities of aggregate gravel of drainage layer were used: 1e-8 m^2 and 1e-9 m^2. In the air-sealed cases air sealing structure consisted 50 mm thick concrete slab.

Studied structures were simulated with different air change rates of replacement air, i.e. the air directly from outdoors to crawl space via adjusted air valves in the foundation wall. Chosen air change rates for replacement air were 0.2, 0.4, 0.6, 0.8, 1.0, 2.0 and 5.0 1/h. National recommendation in Finland for air change rates of crawl space are 0.5 – 1.0 1/h (LVI 06-40064 2004), which are based on study by Airaksinen (2003). Air change rates and volume flows of replacement air corresponding to the air change rates are expressed in Tables 8, 9 and 10.

The smallest air change rate of replacement air (0.2 1/h) was chosen because crawl space should not be ever without any ventilation. In unventilated crawl space cumulates more moist, microbes, radon and other substances that are harmful to health (STUK-A252 2012). Air chance rates 2.0 1/h and 5.0 1/h are used to examine moisture and temperature conditions of the crawl space when air change rate increases to big value. Increasing the air change rate more and more would eventually lead to

situation, where the temperature and humidity conditions of crawl space are equal to outdoor conditions.

3.1 Temperature and humidity fields in ground and foundation structure

Some examples of numerically solved temperature and humidity fields at certain instant are shown in this chapter. In figures 8, 9 and 10 are visualized the temperature fields in the beginning of January of the second simulation year (8772 hours from start of simulation) for cases, where the permeability of gravel was 1e-8 m^2 (Fig. 8) or 1e-9 m^2 (Fig. 9) or the ground was air-sealed (Fig. 10). In figures 11, 12 and 13 are visualized the corresponding relative humidity fields.

As can be seen in figures 8, 9 and 10 the temperature field of ground- and foundation structures are not significantly different. Permeability of aggregate gravel does not thus affect strongly to the temperature field of the aggregate gravel when the pressure difference is moderate. Despite of cold outdoor temperatures in winter, the temperature field below crawl space and ground surrounding near the building is considerably warmer than outdoor temperature. This is obvious and well-known thermal behaviour of ground below a building when there are no airflows in drainage layer, but it was somewhat unexpected that the effect of all-year airflows on ground temperature field is minor. Conclusion is that because of the very low density and specific heat capacity of air compared to solid ground material the flow velocities should be much higher in order to have significant effect on the ground temperatures.

As can be seen in figures 11, 12 and 13 – in contrast to the temperature fields – the corresponding relative humidity fields are significantly different. Conclusion is that the higher the flow velocities

are, the more the depressurization dries the conditions inside drainage gravel in cold periods. When there are no convection (air-sealed case), the moisture at the soil surface diffuses freely to the whole domain, making the relative humidity near 100 % RH everywhere in the drainage layer.

3.2 Hygrothermal conditions in the crawl space

In figures 14, 15 and 16 are visualized the mean monthly temperatures of crawl space for different cases. Mean monthly outdoor temperature (Jokioinen 2004) is also included in figures. Number *a* describes the ratio between volume flow of air through ground (R_{ground}) and flow directly from outdoors (R_{out}) as expressed in equation 12. Air-change rates in the legend are the total air-change rates in crawl space, which contain both volume flows through ground and through adjustable valves.

Figures 14, 15 and 16 indicate that by increasing the volume flow from outdoor the crawl space temperature approaches outdoor temperature. This kind of behavior is of course expected and also noticed earlier by Airaksinen (2003) and Kurnitski (2000) in studies of ventilated but non-depressurized uncovered crawl spaces. Results of uncovered structures and airtight structures are not 100 % comparable to each other concerning of the total air change rate because of slightly different magnitude of total air change rates.

In figures 17, 18 and 19 are visualized the mean monthly values of relative humidity in crawl space for same simulation cases as in figures 14, 15 and 16.

As it can be seen from the figures, the relative humidity in crawl space is very different from outdoor conditions even if the volume flow from outdoors is increased considerably. According to the numerical results, there seems to be two interesting seasonally recurring phases in the behaviour of crawl space: in the fall and winter (from September to March) mean relative humidity in crawl space is clearly at lower level than in outdoors, but in the rest of the year the values are slightly higher but close to outdoor conditions. In airtight case, the monthly mean values of relative humidity are very similar to uncovered cases with the exception that the moisture capacity of concrete moderates the conditions by decreasing highest values and increasing lowest values.

3.3 Depressurization impact on mould growth risk in crawl space

Purpose of this study was find out does depressurization of crawl space decrease or increase risk of mould growth in crawl space compared to outdoor conditions. Studied cases are compared by number of hours when the mould growth is possible in construction materials, i.e. when both relative humidity is $RH \geq 80$ % RH and temperature $T > 0$ °C (Ojanen et al. 2010). This is rough analysis, because the rate of mould growth may be almost negligible when the conditions are near the limit values, but it gives us guiding information in general about the effect of the depressurization on mould growth risk.

In table 11 are shown the calculated number of hours when the mould growth is possible based on heat and moisture conditions of crawl space. As it can be seen from the table, airtightening the crawl space decreases strongly number of hours of the conditions when mould growth is possible. There is also difference between uncovered structures: number of hours of the possible conditions for mould growth is slightly smaller in case where permeability of aggregate gravel is 1e-9 m^2 than in case where permeability is 1e-8 m^2.

In all studied cases the number of hours for possible mould growth increases when air change rate for replacement air increases and the outdoor conditions seem to be more critical for mould growth than conditions in crawl space with any studied air change rate. Conclusion is that if the air leakages from indoor air can be neglected, the depressurization system with moderately adjusted airflow from outdoors does not increase the risk of mould growth in crawl space; converesely, it keeps the conditions very dry during fall and winter. However, according to the results, the safest solution would be covering the crawl space bottom with concrete layer, which moisture capacity has additional positive effect in keeping the crawl space air dry and keeps the crawl space bottom airtight.

4 Conclusions

Aim of this study was to investigate numerically the effect of constant 10 Pa depressurization on hygrothermal conditions and risk of mould growth in typical Finnish crawl space of a detached house. Purpose of the depressurization is to prevent insanitary particles leaking into indoor air and thus to improve the indoor air quality in part of e.g. radon concentration. A finite element based multicomponent hygrothermal model (MCHTM) was compiled in COMSOL Multiphysics, where the effect of convection in drainage layer, heat and moisture transfer in surrounding structures and adjustable air change rate from outdoors was taken into account. Several physical simplifications had to be done because of the limited computational resources and knowledge of materials.

According to the computational results, the conditions in depressurized crawl space (10 Pa pressure difference) are most of the time during the year less favorable for mould growth compared to outdoor conditions, even if the drainage layer permeability is high (1 e-8 m^2) and the soil under the drainage layer is constantly wet. If the permeability of the gravel in drainage layer is smaller, the hygrothermal

conditions become less critical and even less if the crawl space bottom is airtightened with concrete layer. Even though the air flowing through drainage layer may accumulate water vapour from moist soil, the temperature of air increases typically while flowing through ground (depending on the season) and it seems to have more significant effect on the relative humidity in crawl space.

Despite of the simplifications, results of the MCHTM simulations were found to be logical in part of the time-dependent temperature and humidity conditions of the crawl space: in fall and winter outdoor air is colder than ground, and the flowing air in the drainage layer gets warmer and drier before entering the crawl space air. In spring and summer the ground is colder than outdoor air, and the flowing air in drainage layer gets colder, which means also that the relative humidity rises. In general, the possible mould growth in building structures is typically strongest in fall after the summer, when outdoor temperature starts to decrease and relative humidity rises, but because of the thermal inertia of the ground, depressurized crawl space conditions are then quite dry because of the warming effect of ground on the flowing air in drainage layer. However, during summers, the conditions of crawl space are to some extent worse (in part of mould growth) compared to outdoors, because the ground is colder than outdoor air.

5 Discussion

Based on results, general conclusion of this study is that warming up of cold outdoor air during the flow through drainage layer mainly decrease relative humidity of crawl space, although outdoor air can accumulate water vapour from moist foundation soil while flowing through drainage layer. Based on typically warming effect of ground (depending on the season), it seems that the depressurization of crawl space does not have effect that increases risk of mould growth in crawl space. In reality,

however, the flow through drainage layer, can occasionally be much smaller than flows simulated in this study by Darcy's law, because there might be snow, leaves or more dense soil layer on top of the drainage layer. According to the results, however, this would have positive effect on crawl space conditions since the airflow through ground would be lesser. Also, if the depressurization is maintained for years, surface between foundation soil and drainage layer might slowly dry, which would have also positive effect.

Admittedly, the used model lacks the effect of non-zero moisture capacity due to sorption of the gravel in drainage layer. Especially when convection is also present in combined heat and water vapour transport inside porous medium, it should be noted that the pore system may occasionally be in local non-equilibrium, i.e. the temperature of the flowing air may differ locally from the temperature of the solid part of the porous medium. Same is true for the humidity, i.e. relative humidity can have local difference between the flowing air and the pore surfaces. Taking into account this possibility in modeling was concluded to be an unavailable option, because it would require currently unavailable knowledge of interstitial heat and mass transfer coefficients in the porous gravel layer. However, the moisture capacity of gravel, which is washed from dust and consist of large granules, was assumed to be negligible and it was decided that the modelling with this assumption is worthwhile. Occasionally condensing water was also assumed to pour down immediately off the drainage layer due to gravity and adsorb into the base soil, where relative humidity was assumed to be constantly at 100 % RH.

More detailed time-dependent analysis of the mould growth in crawl space according to the numerical results could be done by Finnish mould growth model, which is based on older mould growth model for wooden materials (Hukka & Viitanen 1999), but which also takes into account the sensitivity classes of different building materials for mould growth (Viitanen et al. 2010; Ojanen et al. 2010).

This type of more sophisticated mould risk analysis for depressurized crawl spaces based on results shown in this paper is, however, left for future work. Validity of the used numerical model (MCHTM) and realiability of the conclusions are difficult to evaluate without long-term experimental data and therefore it is suggested that the future studies of depressurized crawl spaces should focus on field measurements in actual depressurized crawl spaces, where also the possible effect of air leakage from indoors are present also. We emphasize, that the results and conclusions in this paper apply for a situation where air leakages from indoors are completely absent. This study was thus not complete analysis of the hygrothermal effects of depressurization on crawl space, and it focused on the questions what happens to the air as it is forced to flow through ground into crawl space. Obviously, if the base floor structure has considerable air leakages the depressurization is not suitable method for ensuring low radon concentrations in indoors if the base floor structure is not airtightened also. However, even if the floor structure is airtight energy-efficiency-wise and in the view of moisture-safety of the crawl space, depressurization system (or other radon preventation system) may be required to keep the radon concentration in indoors at acceptable levels.

References

Airaksinen, M. (2003). Moisture and fungal spore transport in outdoor air-ventilated crawl spaces in a cold climate. Report A7. 2003. Doctoral Thesis. Helsinki University of Technology, Department of Mechanical Engineering, Laboratory of Heating, Ventilating and Air Conditioning, Finland.

C4. (2003). National Building Code of Finland, Energy efficiency: Thermal insulation Guidelines. Ministry of the Environment. Helsinki.

COMSOL Multiphysics (2016). COMSOL Multiphysics Reference Manual 5.2a. COMSOL AB.

Diallo, T.M.O., Collignan, B. & Allard, F. (2013). Analytical quantification of airflows from soil through building substructures. *Building Simulation*, 6:81-94.

Diallo, T.M.O., Collignan, B. & Allard, F. (2015a). Air flow models for sub-slab depressurization systems design. *Building and Environment*, 87:327-341.

Diallo, T.M.O., Collignan, B. & Allard, F. (2015b). 2D Semi-empirical models for predicting the entry of soil gas pollutants into buildings. Building and Environment vol 85, pages 1-16.

Diallo, T.M.O., Collignan, B. & Allard, F. (2017). Analytical quantification of the impact of sub-slab gravel layer on the airflow from soil into building substructures. *Building Simulation*, doi:10.1007/s12273-017-0375-y.

EN ISO 13788:2012. Hygrothermal performance of building components and building elements. internal surface temperature to avoid critical surface humidity and interstitial condensation. Calculation methods. European Committee for Standardization.

Gadgil, A.J. (1992). Models of radon entry. *Radiation Protection Dosimetry,* vol. 45:373-379.

Hagentoft C-E. (2001). Introduction to building physics. Studentlitteratur, Lund, Sweden.

Henschel, D. Bruce (1992). Indoor Radon Reduction in Crawl-space Houses: a Review of Alternative Approaches. *Indoor Air*, 2:272-287.

Hukka, A. & Viitanen, H. (1999). A Mathematical Model of Mould Growth on Wooden Material. *Wood Science and Technology*, 33:475-485.

Jiranek, M. & Svoboda, Z. (2007). Numerical modelling as a tool for optimisation of sub-slab depressurisation systems design. *Building and Environment*, 42: pages 1994-2003.

Jokioinen (2004). Test year climate data Jokioinen 2004. Finnish meteorological institute. Available at http://ilmatieteenlaitos.fi/Rakennusfysiikan-testivuodet-nykyilmastossa. Accessed 19 Feb 2017. (in Finnish).

Keskikuru T, Kokotti H., Lammi S., and Kalliokoski P. (1999). How did wind affect the radon entry into seven detached houses. In: Proceedings of Radon in the living environment 19-23 April, 309-319.

Keskikuru T., Kokotti H., and Kalliokoski P. (2000a). Pressure differences in seven supply and exhaust ventilated houses. *Proceedings of Healthy Buildings*, 3, 91-97.

Keskikuru T., Kokotti H., Lammi S., and Kalliokoski P. (2000b). Variation of radon entry rate into two detached houses. *Atmospheric Environment*, 34:4819-4828.

Keskikuru T., Kokotti H., Lammi S., and Kalliokoski , P. (2001). Effect of various factors on the radon entry rate into two different types of houses. *Building and Environment*. 36:1091-1098.

Künzel, H. (1995). Simultaneous Heat and Moisture Transport in Building Components – One- and two-dimensional calculation using simple parameters. Doctoral thesis, Fraunhofer Institute of Building Physics. Holzkirchen, Germany.

Kurnitski, J. (2000). Humidity control in outdoor-air-ventilated crawl spaces in cold climate by means of ventilation, group covers and dehumidification. Report A3. 2000. Doctoral thesis. Helsinki University of Technology, Department of Mechanical Engineering, Laboratory of Heating, Ventilating and Air Conditioning, Helsinki.

Leivo, V & Rantala, J. (2001). The moisture behavior of the base floor structures. Tampere University of Technology. Department of Civil Engineering. Research report 106. (in Finnish)

LVI 06-40064 (2004). A functioning crawl space. Information grain card. Publication, Rakennustieto. (in Finnish).

Matilainen, M. & Kurnitski, J. (2003). Moisture conditions in highly insulated outdoor ventilated crawl spaces in cold climates. Energy and Buildings. Volume 35, Issue 2. Pages 175-187.

Nazaroff, W.W. (1992). Radon transport from soil to air. *Reviews of Geophysics*, 30:137-160.

Nusser, B. & Teibinger, M. (2012). Coupled Heat and Moisture Transfer in Building Components – Implementing WUFI Approaches in COMSOL Multiphysics. Proceedings of the 2012 COMSOL Conference, Milan, Italy.

Ojanen, T., Viitanen, H., Peuhkuri, R., Lähdesmäki, K., Vinha, J. & Salminen, K. (2010). Mold Growth Modeling of Building Structures Using Sensitivity Classes of Materials. Proceedings of Thermal Performance of the Exterior Envelopes of Whole Buildings XI, Clearwater Beach, Florida, USA, December 5–9. ASHRAE, DOE, ORNL, Session II-B, 10 p.

Rantala, J. & Leivo, V. (2007). Thermal and moisture parameters of a dry coarse-grained fill or drainage layer. *Construction and Building Materials*, 21:1726-1731.

RIL 107 (2012). Water and moisture proofing of buildings. Technical report. Finnish Association of Civil Engineers (Suomen Rakennusinsinöörien Liitto RIL ry). (in Finnish).

Riley, W.J., Gadgil, A.J., Bonnefous, Y.C. & Nazaroff, W.W. (1996). The effect of steady winds on radon-222 entry from soil into houses. *Atmospheric Environment*, 30:1167-1176.

STUK-A252 Arvela H, Holmgren O, Reisbacka H. (2012). Indoor radon mitigation. Helsinki. (In Finnish).

Viitanen, H. Vinha, J., Salminen, K., Ojanen, T., Peuhkuri, R., Paajanen, L. & Lähdesmäki, K. (2010). Moisture and Bio-deterioration Risk of Building Materials and Structures. *Journal of Building Physics*, 33(3):201-224.

Vinha, J., Laukkarinen, A., Mäkitalo, M., Nurmi, S., Huttunen, P., Pakkanen, T.,Kero, P., Manelius, E., Lahdensivu, J., Köliö, A., Lähdesmäki, K., Piironen,J., Kuhno, V., Pirinen, M., Aaltonen, A., Suonketo, J., Jokisalo, J., Teriö,O., Koskenvesa, A. & Palolahti, T. (2013). Effects of climate change and increasing of thermal insulation on moisture performance of envelope assemblies and energy consumption of buildings. Tampere University of Technology. Department of Civil Engineering. Research report 159. 354 p. + 43 p. app. (in Finnish)

Williams Portal, N. (2011). Evaluation of heat and moisture induced stress and strain of historic building materials and artefacts. Master's Thesis. Chalmers University of Technology, Gothenburg, Sweden.

Zeng, Z. & Grigg, R. (2006). A Criterion for Non-Darcy Flow in Porous Media. Transport in Porous Media (2006) 63: 57-69.

Zienkiewicz, O.C., Nithiarasu, P. & Taylor, R.L. (2013). The Finite Element Method: The Finite Element Method for Fluid Dynamics 7th edition. Elsevier Science.

Table 1 Permeabilities and grain size ranges of typical Finnish gravel aggregates (STUK A-252 2012).

Aggregate name	**Permeability (m^2) (order of magnitude)**	**Size range (mm)**
Fine sand	1e-11	0.06-0.2
Medium sand	1e-10	0.2-0.6
Coarse sand	1e-9	0.6-2.0
Fine gravel	1e-9	2-6
Medium gravel	1e-8	6-20
Coarse gravel	1e-7	20-60

Table 2 Water vapor sorption isotherm of concrete K3 (Vinha et al. 2013).

RH	[RH %]	0	5	10	15	20	30	40	50	60	70	80	90	95	100
w	[kg/m^3]	0	27	32	34	35	37	40	48	58	72	85	100	118	150

Table 3 Liquid transport coefficient in function of moisture content of concrete K3 (Vinha et al. 2013).

w [kg/m^3]	0	72	85	100	118
D_w [m^2/s]	0	7,40E-11	2,50E-10	1,00E-09	1,20E-09

Table 4 Thermal conductivity of concrete as a fuction of moisture content (Vinha et al. 2013).

Moisture content	*w* [kg/m^2]	0	180
Thermal conductivity	λ [W/(m·K)]	1,6	2,602

Table 5 Function of moisture content of XPS- thermal insulation (Vinha et al. 2013).

RH	[%]	0	35	50	70	80	90	98	100
w	[kg/m^3]	0	0,14	0,17	0,2	0,21	0,28	0,36	45

Table 6 Other thermal material properties of of XPS- thermal insulation (Vinha et al. 2013).

Liquid transport coefficient	D_w [m^2/s]	0
Thermal conductivity	λ [W/(m·K)]	0,037
Soecific heat capacity	c_p [J/(kg·K)]	1500
Density	ρ [kg/m^3]	60

Table 7 Other construction material thermal material properties which was used in study.

Thermal conductivity λ [W/(m·K)]	Density ρ [kg/m^3]	Specific heat capacity c_p [J/(kg·K)]	

Aggregate gravel	1	1800	900	Leivo & Rantala (2001)
Foundation soil	1	1800	900	Leivo & Rantala (2001)
Concrete K3	1,6	2300	850	Vinha et al. (2013)
Expanded clay aggregate	0,25	700	1000	C4 (2003)
EPS	0,039	15	1300	Vinha et al. (2013)

Table 8 Used volume flows and air change rates (ACR) in the simulation when concrete air sealed structure.

R_{out} (m^3/s)	n (1/h)
0.0058	0.2
0.0115	0.4
0.0173	0.6
0.0230	0.8
0.0288	1.0
0.0576	2.0
0.1439	5.0

Table 9 Volume flows and air change rates (ACR) in the simulation when aggregate gravel permeability was 1e-8 m^2.

R_{out} (m^3/s)	R_{ground} (m^3/s)	R_{tot} (m^3/s)	n (1/h)	a (-)
0.0058	0.028	0.0336	1.2	4.8
0.0115	0.028	0.0393	1.4	2.4
0.0173	0.028	0.0451	1.6	1.6
0.023	0.028	0.0509	1.8	1.2
0.0288	0.028	0.0566	2.0	1.0
0.0576	0.028	0.0854	3.0	0.5
0.1439	0.028	0.1717	6.0	0.2

Table 10 Volume flows and air change rates (ACR) in the simulation when aggregate gravel permeability was 1e-9 m^2.

R_{out} (m^3/s)	R_{ground} (m^3/s)	R_{tot} (m^3/s)	n (1/h)	a (-)
0.0058	0.0028	0.0085	0.30	0.48
0.0115	0.0028	0.0143	0.50	0.24
0.0173	0.0028	0.0201	0.70	0.16
0.0230	0.0028	0.0258	0.90	0.12
0.0288	0.0028	0.0316	1.10	0.10
0.0576	0.0028	0.0603	2.10	0.05
0.1439	0.0028	0.1467	5.10	0.02

Table 11 Number of hours of the favourable conditions to mould growth in varying air change rates and studied structures.

	Number of hours of the possible conditions for mould growth		
	Uncovered structures		Airtight structure
Air change rate for replacement air (1/h)	Permeability 1e-8 m^2	Permeability 1e-9 m^2	Concrete slab 50 mm
0.2	5782	5551	1573
0.4	5665	5238	3548
0.6	5609	5203	3971
0.8	5605	5151	4457
1.0	5582	5136	4702
2.0	5486	5122	4911
5.0	6144	5820	5016
Outdoor conditions	7157	7157	7157

Fig. 1 Example figure of uncovered ground and foundation structure.

Fig. 2 Example figure of airtight ground and foundation structure.

Fig. 3 The whole geometry of studied ground and foundation structures.

Fig. 4 Visualization of total velocity in the gravel when constant 10 Pa depressurization (permeability 1e-9 m^2).

Fig. 5 Illustration of energy and mass balances in lumped system model of crawl space.

Fig. 6 Outdoor temperature (°C) and relative humidity (% RH) in Jokioinen 2004 - weather data (Vinha et al. 2013).

Fig. 7 Example of used mesh structure for drainage layer and foundation soil in COMSOL Multiphysics.

Fig. 8 Temperature field surrounding the uncovered crawl space (aggregate gravel permeability 1e-8 m^2) in beginning of the January of the second simulation year (8772 hour from start of simulation).

Fig. 9 Temperature field surrounding the uncovered crawl space (aggregate gravel permeability 1e-9 m^2) in beginning of the January of the second simulation year (8772 hour from start of simulation).

Fig. 10 Temperature field surrounding the concrete air-sealed crawl space in beginning of the January of the second simulation year (8772 hour from start of simulation).

Fig. 11 Relative humidity field surrounding the uncovered crawl space (aggregate gravel permeability 1e-8 m^2) in beginning of the January of the second simulation year (8772 hour from start of simulation).

Fig. 12 Relative humidity field surrounding the uncovered crawl space (aggregate gravel permeability 1e-9 m^2) in beginning of the January of the second simulation year (8772 hour from start of simulation).

Fig. 13 Relative humidity field surrounding the concrete air-sealed crawl space in beginning of the January of the second simulation year (8772 hour from start of simulation).

Fig. 14 Mean monthly temperatures (°C) of uncovered crawl space (aggregate gravel permeability is 1e-8 m^2).

Fig. 15 Mean monthly temperatures (°C) of uncovered crawl space (aggregate gravel permeability is 1e-9 m^2).

Fig. 16 Mean monthly temperatures (°C) of crawl space where ground is air-sealed with concrete layer.

Fig. 17 Mean monthly relative humidity (-) of uncovered crawl space (aggregate gravel permeability is 1e-8 m^2).

Fig. 18 Mean monthly relative humidities (-) of uncovered crawl space (aggregate gravel permeability 1e-9 m^2).

Fig. 19 Mean monthly relative humidities (-) of crawl space where ground is air-sealed with concrete layer.

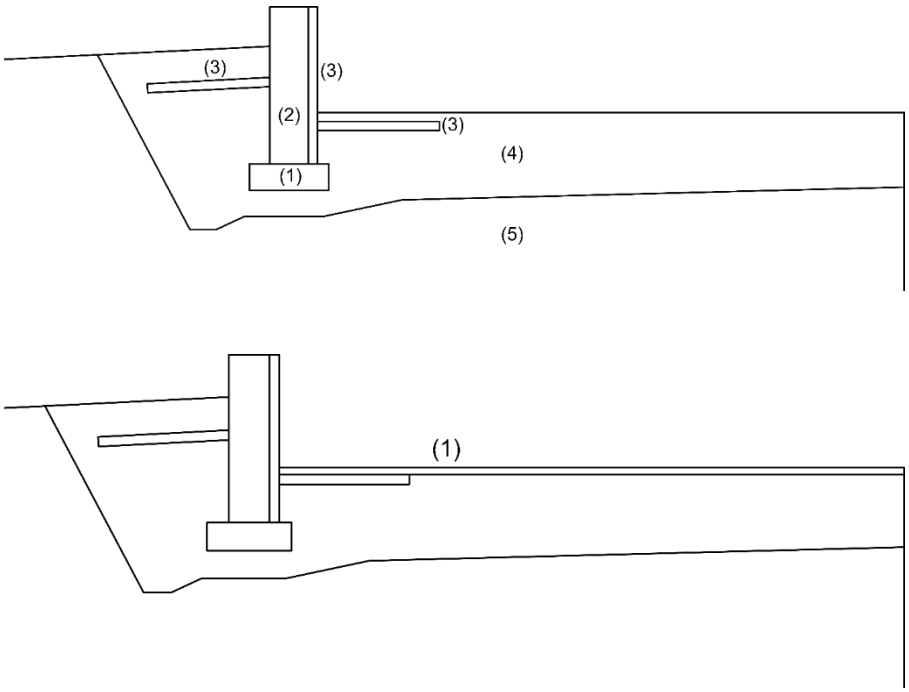

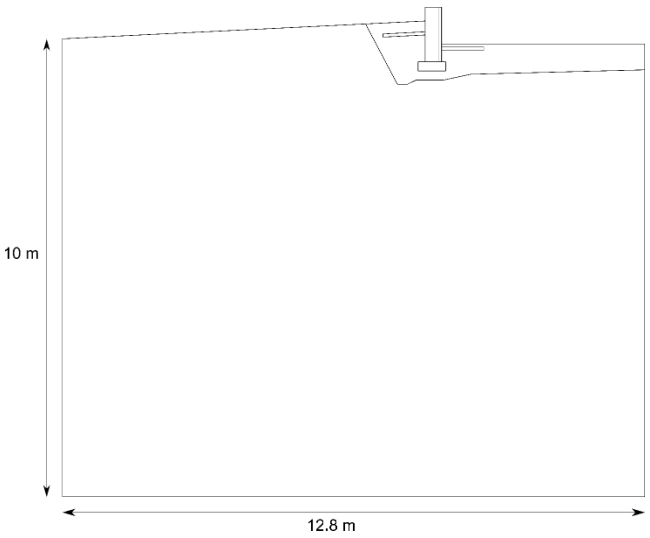

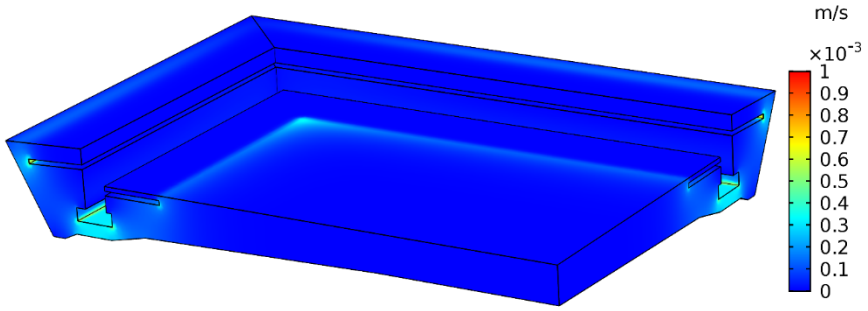

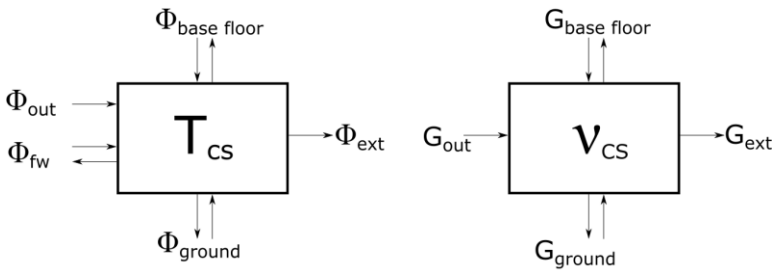

Φ heat flow [W]

G mass flow [kg/s]

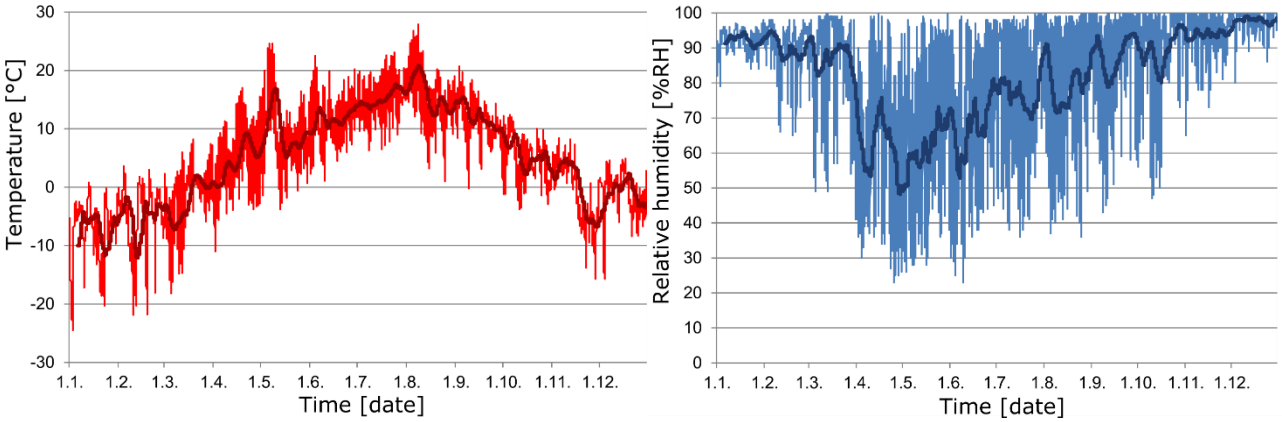
Temperature [°C]
30
20
10
0
-10
-20
-30
1.1. 1.2. 1.3. 1.4. 1.5. 1.6. 1.7. 1.8. 1.9. 1.10. 1.11. 1.12.
Time [date]
Relative humidity [%RH]
100
90
80
70
60
50
40
30
20
10
0
1.1. 1.2. 1.3. 1.4. 1.5. 1.6. 1.7. 1.8. 1.9. 1.10. 1.11. 1.12.
Time [date]

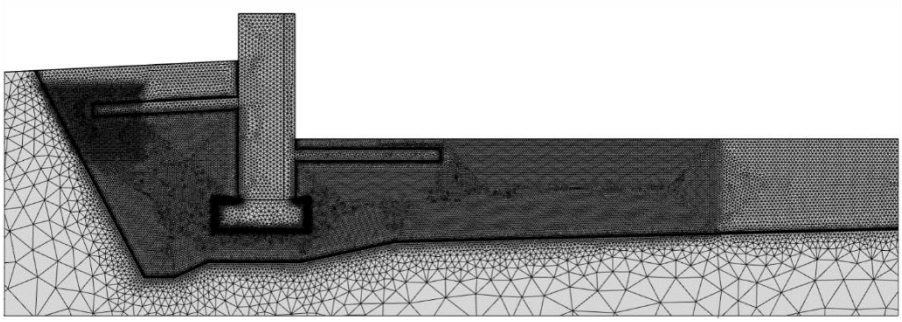

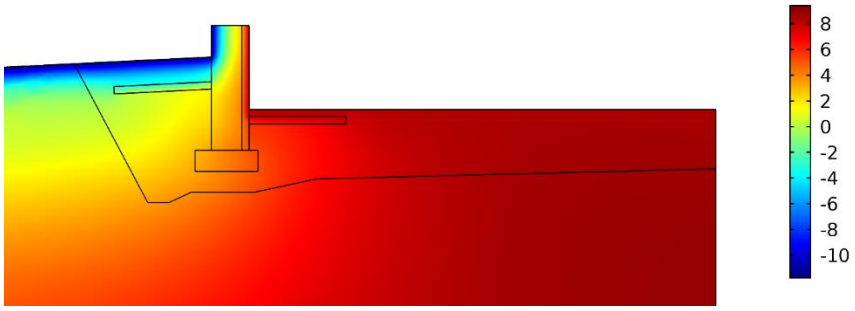
8
6
4
2
0
-2
-4
-6
-8
-10

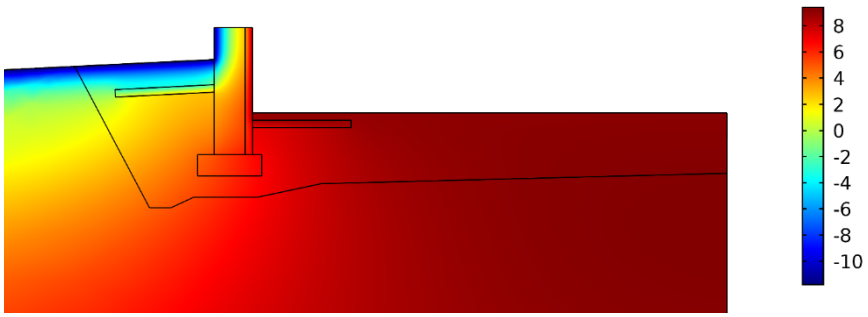
8
6
4
2
0
-2
-4
-6
-8
-10

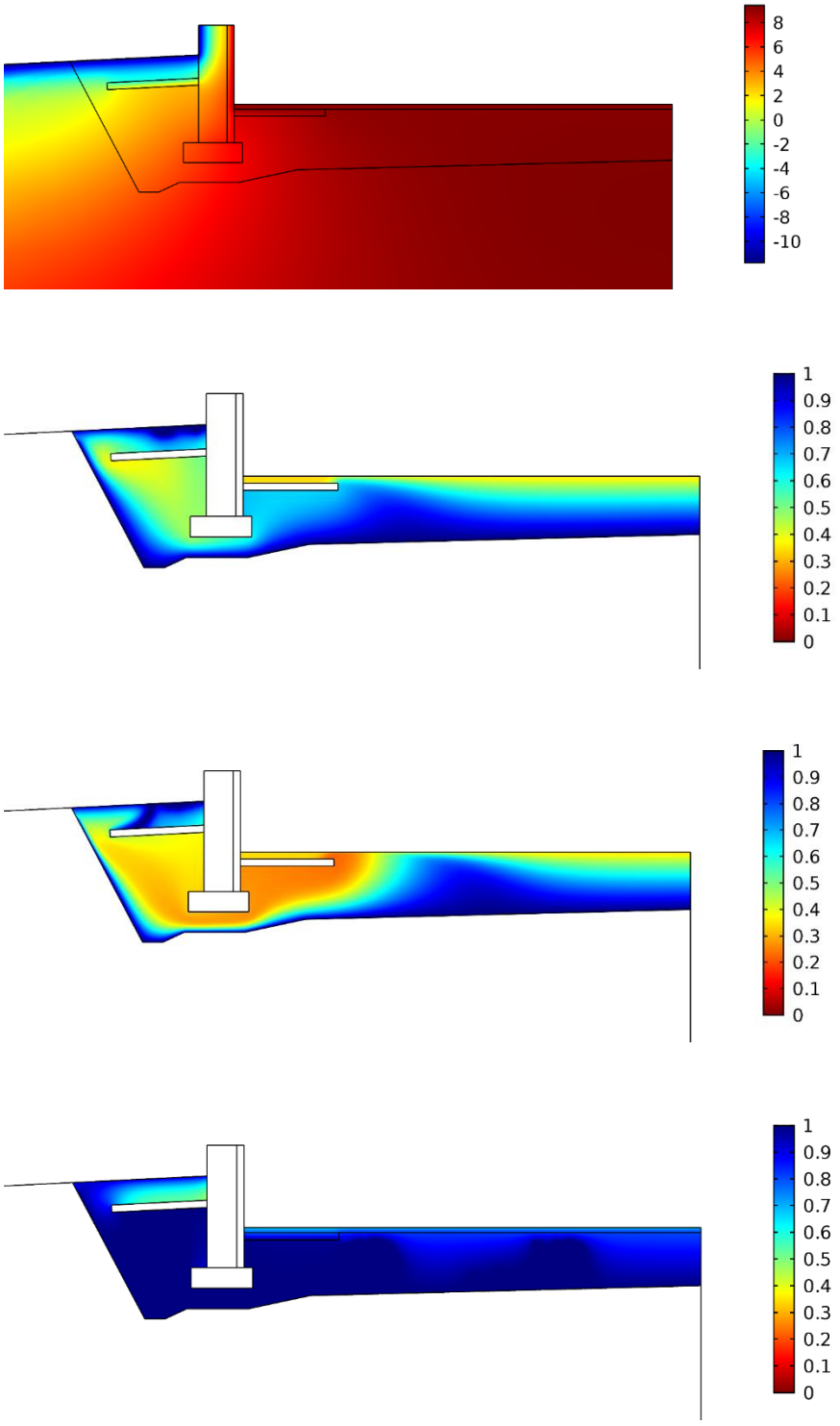
8
6
4
2
0
-2
-4
-6
-8
-10
1
0.9
0.8
0.7
0.6
0.5
0.4
0.3
0.2
0.1
0
1
0.9
0.8
0.7
0.6
0.5
0.4
0.3
0.2
0.1
0
1
0.9
0.8
0.7
0.6
0.5
0.4
0.3
0.2
0.1
0

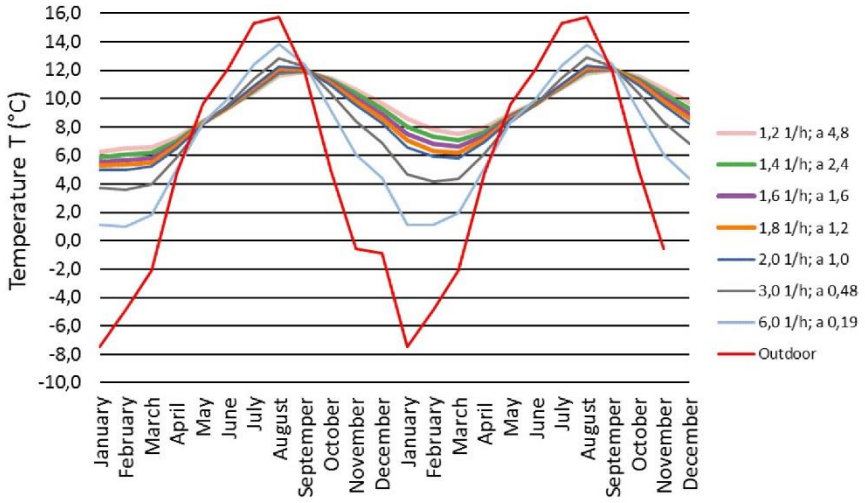
Temperature T (°C)
16,0
14,0
12,0
10,0
8,0
6,0
4,0
2,0
0,0
-2,0
-4,0
-6,0
-8,0
-10,0
January
February
March
April
May
June
July
August
Septemper
October
November
December
1,2 1/h; a 4,8
1,4 1/h; a 2,4
1,6 1/h; a 1,6
1,8 1/h; a 1,2
2,0 1/h; a 1,0
3,0 1/h; a 0,48
6,0 1/h; a 0,19
Outdoor

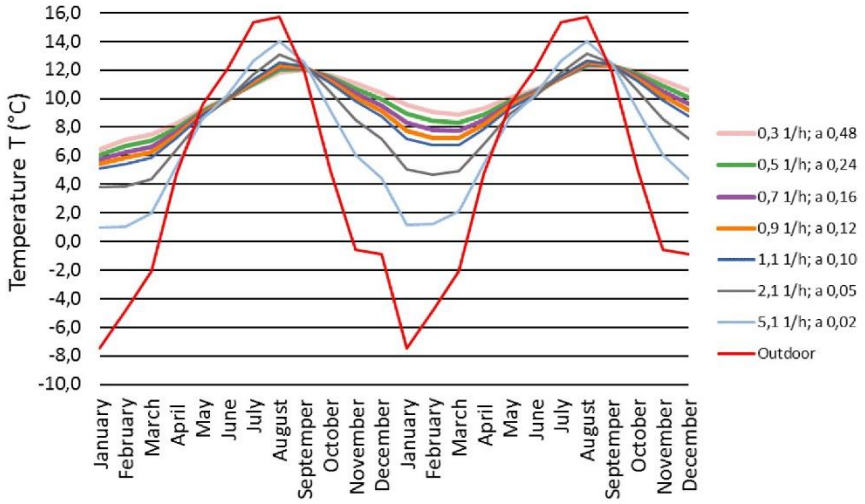
Temperature T (°C)
16,0
14,0
12,0
10,0
8,0
6,0
4,0
2,0
0,0
-2,0
-4,0
-6,0
-8,0
-10,0
January
February
March
April
May
June
July
August
Septemper
October
November
December
0,3 1/h; a 0,48
0,5 1/h; a 0,24
0,7 1/h; a 0,16
0,9 1/h; a 0,12
1,1 1/h; a 0,10
2,1 1/h; a 0,05
5,1 1/h; a 0,02
Outdoor

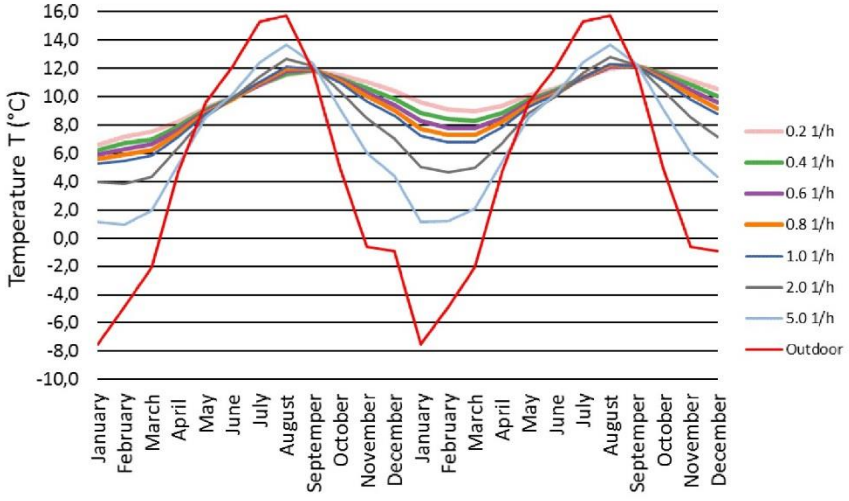
Temperature T (°C)
16,0
14,0
12,0
10,0
8,0
6,0
4,0
2,0
0,0
-2,0
-4,0
-6,0
-8,0
-10,0
January
February
March
April
May
June
July
August
Septemper
October
November
December
0.2 1/h
0.4 1/h
0.6 1/h
0.8 1/h
1.0 1/h
2.0 1/h
5.0 1/h
Outdoor

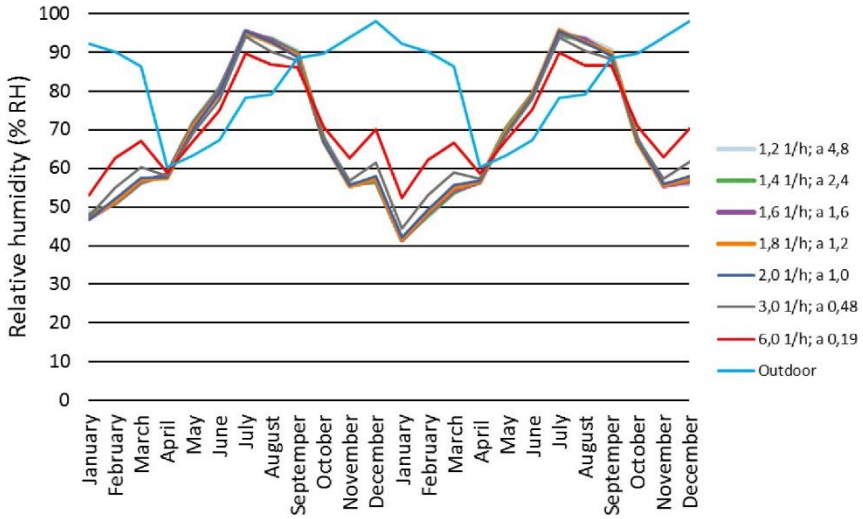
Relative humidity (% RH)
100
90
80
70
60
50
40
30
20
10
0
January
February
March
April
May
June
July
August
Septemper
October
November
December
1,2 1/h; a 4,8
1,4 1/h; a 2,4
1,6 1/h; a 1,6
1,8 1/h; a 1,2
2,0 1/h; a 1,0
3,0 1/h; a 0,48
6,0 1/h; a 0,19
Outdoor

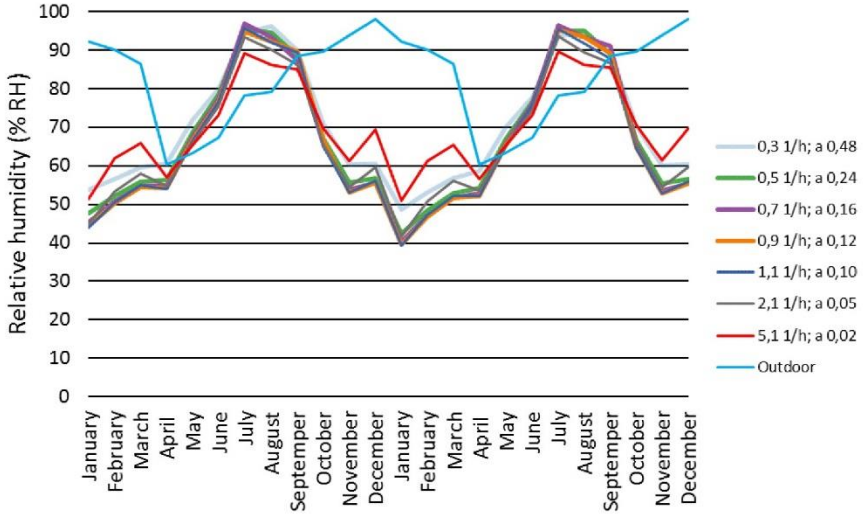
Relative humidity (% RH)
100
90
80
70
60
50
40
30
20
10
0
January
February
March
April
May
June
July
August
Septemper
October
November
December
0,3 1/h; a 0,48
0,5 1/h; a 0,24
0,7 1/h; a 0,16
0,9 1/h; a 0,12
1,1 1/h; a 0,10
2,1 1/h; a 0,05
5,1 1/h; a 0,02
Outdoor

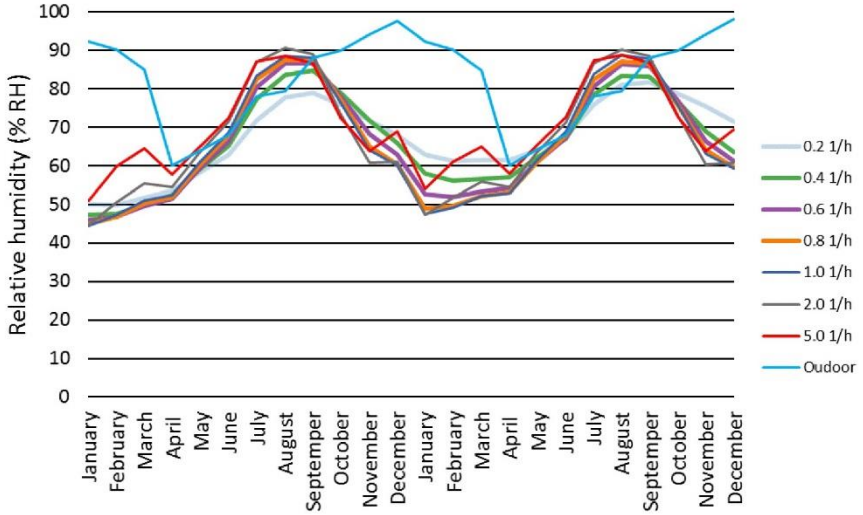
Relative humidity (% RH)
100
90
80
70
60
50
40
30
20
10
0
January
February
March
April
May
June
July
August
Septemper
October
November
December
0.2 1/h
0.4 1/h
0.6 1/h
0.8 1/h
1.0 1/h
2.0 1/h
5.0 1/h
Oudoor